Journal of Applied Fluid Mechanics, Vol. 17, No. 3, pp. 658-671, 2024.
Available online at www.jafmonline.net, ISSN 1735-3572, EISSN 1735-3645.
https://doi.org/10.47176/jafm.17.3.2134

Impact of Magnetic Fields and Fins on Entropy Generation, Thermal, and Hydrodynamic Performance in the Ferrofluids Flow within a Mini Channel

L. Boutas[1], M. Marzougui[2], J. Zinoubi[1, 2†] and S. Gannouni[1]

[1] *Faculty of Sciences of Tunis, Department of Physics, Laboratory of Energizing and Thermal and Mass Transfer, University of Tunis El-Manar, Tunis, Tunisia*
[2] *Department of Physics, Preparatory Institute of the Engineers Studies of El-Manar, University of Tunis El-Manar, Tunis, Tunisia*

†Corresponding Author Email: jamil.zinoubi@ipeiem.utm.tn

ABSTRACT

The present work reports a CFD study of the magneto-convection of a ferrofluid $(Fe_3O_4/water)$ circulating in a mini-channel under the influence of different vortex generators (fins and permanent magnets). The lower surface of the mini-channel is maintained at a constant temperature, while the upper surface is thermally insulated. The influence of fins, magnetic field intensity, and Reynolds number on the thermal and dynamic characteristics of the flow was numerically investigated using the finite volume method. The obtained results show that the coexistence of these two types of vortex generators considerably affects the flow structure; Entropy generation and heat transfer rate. Finally, the analysis of the different results shows that the concurrent presence of both the magnetic field and the fins results in a notably more efficient system. Using magnetic sources and fins simultaneously in a system with an intense magnetic field and a low Reynolds number can lead to a large gain in heat transfer.

Article History

Received July 6, 2023
Revised October 13, 2023
Accepted October 15, 2023
Available online January 1, 2024

Keywords:

Ferrofluids
Vortex generator
Magnetic source
Magnetic body force
Entropy generation

1. INTRODUCTION

With the development of thermal systems, improving the efficiency of convective exchangers has become a significant challenge. Including, the increase in the exchange surfaces such as using fins (Sachdeva et al., 2010; Gupta & Kasana, 2012). This is a passive technique based on the use of vortex generators to enhance the flow turbulence and therefore leads to improve the heat transfer efficiency. Several researchers, (Akbari et al., 2015; Ghale et al., 2015; Karimipour et al., 2015) conducted a numerical investigation of the impact of rectangular fins on the heat transfer performance of a nanofluids circulating in a rectangular microchannel. They found that the presence of the fins leads to a significant improvement in heat transfer accompanied by an increase in friction coefficients. Similarly, Manca et al. (2012) studied the turbulent heat transfer of nanofluid $(Ag/water)$ in a channel with the presence of the fins under a constant heat flux. They showed that increasing of Reynolds number and the volume fraction of the considered nanoparticles leads to an improvement in heat transfer. Pishkar and Ghasemi (2012) carried out a numerical study on the thermal performance of a nanofluid $(Cu/water)$ using two fins mounted on the lower wall of a horizontal channel using pure water as a cooling fluid. The findings from this study indicate that the heat transfer rate is notably influenced by the spacing between the fins. Particularly, at higher Reynolds numbers, the impact of the nanofluids volume fraction on enhancing heat transfer becomes more pronounced.

However, most research conducted on nanofluids has highlighted potential challenges, particularly those related to sedimentation and agglomeration. To overcome this problem, the idea was born of using magnetic nanoparticles in conjunction with an external magnetic field. This magnetic field will control the dispersion and movement of the nanoparticles. This exclusive feature can potentially be used in several areas. They find diverse applications in technology, biology, and medicine, as well as contribute to thermal science and engineering research, among other fields (Scherer & Figueriedo, 2005)… etc. In this context, we can distinguish several studies in the literature that have used an active technique of vortex generators to enhance heat transfer performance such as the use of a ferrofluid subject to the impact of an external magnetic field, Wang (2005) and Amani et al. (2018). Ferrofluids are magnetic fluids synthesized in the form of stable colloidal suspensions of iron oxide nanoparticles (Fe_3O_4). These nanoparticles are usually coated with a stable surfactant suitable for the type of liquid which prevents the

Nomenclature

$\boldsymbol{B}$	magnetic induction
B_e	Bejan number
C_p	heat capacity
d	fins height
D	mini-channel height
D_h	hydraulics diameter
$\boldsymbol{F}_K$	Kelvin body force
$h(x)$	local heat transfer coefficient
$\boldsymbol{H}$	magnetic field
$\bar{\bar{I}}$	identity tensor
k	thermal conductivity
l	fins and magnets width
L	mini-channel length
$\boldsymbol{M}$	magnetization
Nu	Nusselt number
Nu_{Ave}	average Nusselt number
Nu_0	Nusselt number for $B = 0G$
Re	Reynolds number
S	total entropy generation
$\mathcal{S}_{\mathrm{F}}$	entropy generation due to magnetic field
$\mathcal{S}_{\mathrm{HT}}$	entropy generation due to heat transfer
$\mathcal{S}_{\mathrm{M}}$	entropy generation due to friction
T	temperature
T_0	ambient temperature
T_h	hot wall temperature
T_{in}	inlet temperature
U	velocity in x direction
$\boldsymbol{u}$	velocity vector
V	velocity in the y-direction
x, y	Cartesian coordinates

Greek symbols:

φ	volume fraction
$\bar{\bar{\tau}}$	stress tensor
χ_m	magnetic susceptibility
χ_0	differential magnetic susceptibility
ρ	density
μ	magnetic viscosity
$\boldsymbol{\nabla}$	Nabla operator
μ_0	permeability of free space ($4\pi 10^{-7}$)
β	volumetric expansion coefficient
δ	Kronecker's symbol

Indexes

f	fluid
nf	nanofluid
Ave	average
p	nanoparticle
in	*Inlet*
w	bottom surface

agglomeration of the nanoparticles by overcoming the attractive Van der Waals forces between the nanoparticles.

Numerous researchers, including Lajvardi et al. (2010); Motozawaa et al. (2010); Ghofrani et al. (2013); and Azizian et al. (2014) have conducted studies investigating the impact of a magnetic field on heat transfer and pressure drop in ferrofluid flows. Their investigations revealed an enhancement in both heat transfer coefficients and pressure drops as the magnetic field intensity increased. In addition, Sadeghinezhad et al. (2017) conducted experimental research on the influence of permanent magnets on heat transfer in graphene-magnetite hybrid nanofluids; they found an impressive 82% increase in convective heat transfer. Xuan et al. (2007) conducted a numerical investigation to explore the impact of the orientation and strength of the magnetic field gradient on the convective flow of ferrofluid within a micro-channel. Their findings primarily emphasized that heat transfer rates experience significant enhancement when the magnetic field and the temperature gradient are in the same direction. In a study by Aminfar et al. (2013), they conducted a numerical analysis to characterize the thermal performance of a ferrofluid inside a vertical rectangular pipe under the influence of a non-uniform transverse magnetic field. Their investigation revealed that the transverse magnetic field had a noticeable impact on the ferrofluid flow throughout the pipe's length. Interestingly, they showed that the emergence of a pair of vortices enhanced the heat exchange while preventing the sedimentation of nanoparticles. Sheikholeslami and Ganji (2017, 2018) and Sheikholeslami et al. (2018, 2019), have investigated the impact of an external magnetic field on the behavior of ferrofluid flow $(Fe_3O_4/water)$ under various configurations using the finite element method. They observed that nanoparticle dispersion leads to an enhanced heat transfer rate, accompanied by a reduction in entropy generation. Furthermore, their research indicated that the intensification of the magnetic fields reduced temperature and velocity gradients. It was also observed that the Nusselt number increases with buoyancy forces and decreases with Lorentz forces. In their study, Mousavi et al. (2019), conducted a study on channels with flat and corrugated walls; their findings indicated that the magnetic field's impact on flow structure and heat transfer was more pronounced in channels with corrugated walls. The application of the magnetic field effectively eliminated surface ripples and redirected the horizontal recirculation zone, leading to an enhanced convective heat exchange.

A numerical study was carried out by Mechighel et al. (2009) to explore the impact of a horizontal magnetic field applied to a three-dimensional floating flow within a parallelepiped box on the stability properties of the flow. The results obtained show that in the absence of a magnetic field and for relatively low values of the Rayleigh number, a stable and symmetrical flow field is obtained with 3D effects limited to the water surface. Tari and Mehrtash (2013) carried out a numerical study on the effect of the heat sink orientations with a parallel arrangement of vertical fins of a rectangular section on a vertical base on the heat transfer rate. The simulation outcomes clearly show that the geometric parameters have a substantial impact on the heat transfer rate. Ragoju and Shekhar (2020) studied both linear and nonlinear stability in magneto-convection within a porous medium with constant vertical magnetic field.

Table 1 Thermo-physical properties

Properties	Water	$Fe_3($
Density $(kg.m^{-3})$	997.1	520(
Heat capacity $(J.kg^{-1}.K^{-1})$	4179	670
Thermal conductivity $(W.m^{-1}.K^{-1})$	0.613	6
Viscosity $(kg.m^{-1}.s^{-1})$	0.003	–
Electrical conductivity $[\Omega^{-1}.m^{-1}]$	0.050	25

Their findings revealed that the thermal Prandtl number has the effect of augmenting heat transfer, whereas the magnetic Prandtl number and the Chandrasekhar number have the opposite effect.

Considering this bibliographical synthesis, the magnetic field and the fins seem to have a considerable influence on the flow characteristics as well as the heat transfer. Evidently, the ferrofluids significantly improve the heat transfer capabilities because the magnetic field applied in the system manages the distribution of nanoparticles. Therefore, the aim of this study is to conduct a numerical investigation into the heat transfer generated by the flow of a ferrofluid ($Fe_3O_4/water$) under the influence of five fins and five magnetic sources.

2. PROBLEM DESCRIPTION

2.1 Geometrical Details

The present work is a numerical investigation of forced convection of a ferrofluid ($Fe_3O_4/water$) circulating in a two-dimensional channel of height D and length L with uniform inlet velocity and temperature. The bottom surface is heated with a uniform temperature T_h while the upper wall is thermally insulated. According to figure1 four different configurations are considered in the numerical simulations: $(Case\ A)$ is a simple mini-channel of dimensions $L \times D$ (length × height). $(Case\ B)$ is a mini-channel with five rectangular fins $(l \times d)$ mounted on the lower wall. $(Case\ C)$ presents a mini-channel with five pairs of magnets located near the upper and lower surfaces. $(Case\ D)$ presents a mini-channel with five fins mounted on the bottom wall of the superimposed mini-channel with five pairs of magnets in an alternating manner. The thermo-physical properties are illustrated in Table 1.

2.2 Mathematical Models

2.2.1 Magnetic Body Force

The ferrofluid is assumed to be electrically nonconducting since the magnetic nanoparticles are coated with an insulating material, such as a surfactant or a polymer that insulates them from each other, which can reduce electrical conductivity (Ganguly et al., 2004a, b), and Maxwell's equations reduce to:

$$\boldsymbol{\nabla}.\boldsymbol{B} = 0 \tag{1}$$

$$\boldsymbol{\nabla} \wedge \boldsymbol{H} = \boldsymbol{0} \tag{2}$$

Based on the Maxwell's equation **B** is related to **H** and **M** as follows:

$$\boldsymbol{B} = \mu_0(\boldsymbol{M} + \boldsymbol{H}) \tag{3}$$

Where $\boldsymbol{B}$ is the magnetic induction vector, $\boldsymbol{H}$ is the magnetic field vector, and $\boldsymbol{M}$ is the magnetization vector.

Assuming that the magnetization vector is aligned with the magnetic field vector:

$$\boldsymbol{M} = \chi_m\, \boldsymbol{H} \tag{4}$$

Where χ_m is the magnetic susceptibility (Ganguly et al. 2004a, b):

$$\chi_m(T) = \frac{\chi_0}{1 + \beta(T - T_0)} \tag{5}$$

From the previous equations, the force of the magnetic body force can be expressed as follows:

$$\boldsymbol{F_k} = (\boldsymbol{M}.\boldsymbol{\nabla})\boldsymbol{B} = \tfrac{1}{2}\mu_0\chi_m(1+\chi_m)\boldsymbol{\nabla}\,(\boldsymbol{H}.\boldsymbol{H}) + \mu_0\chi_m\boldsymbol{H}\big((\boldsymbol{H}.\boldsymbol{\nabla})\chi_m\big) \tag{6}$$

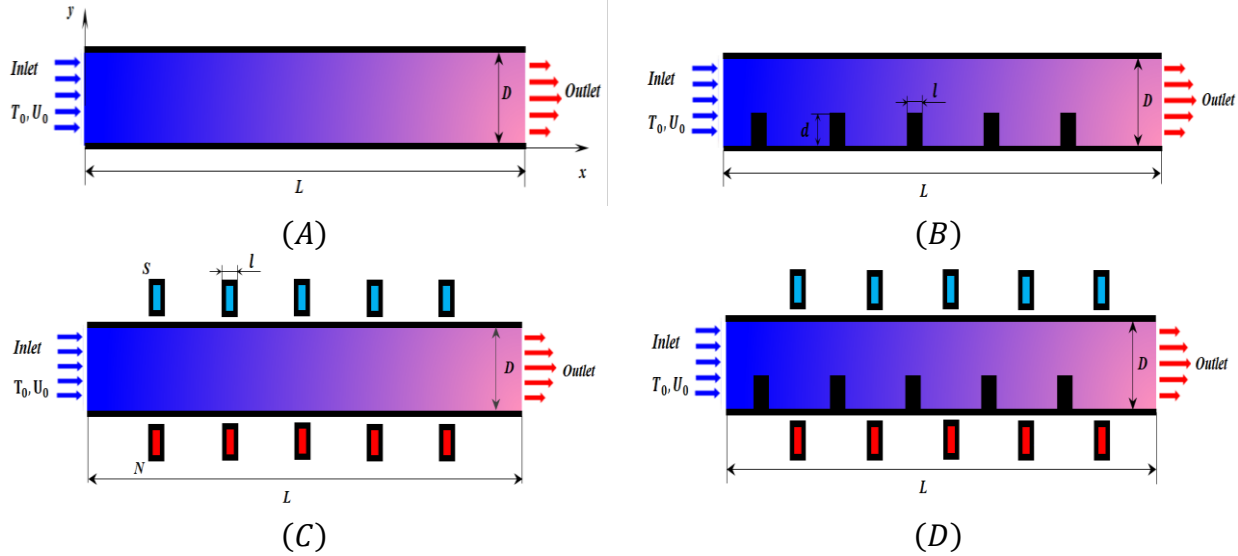

Fig. 1 Physical model

The created magnetic field is almost uniform, which means that the first term is negligible. Strength $\boldsymbol{F}_k$ will only have a uniform component in the y direction (Ganguly et al. 2004a, b):

$$F_k = \mu_0 \chi_m(\boldsymbol{H}^2) \frac{-\chi_0 \beta}{[1+\beta(T-T_0)]^2} \frac{dT}{dy} \tag{7}$$

2.2.2 The Governing Equations

The choice of the steady state for writing the governing equations of a mini heat exchanger, without loss of generality, is grounded in two main considerations. First, it is based on the thermal stability of the system. Second, the time required to reach a steady state is generally relatively short compared to the characteristic times of the system. Consequently, adopting a steady-state approach does not sacrifice result accuracy, streamlining calculations and expediting solution derivation. In mini-channels, the fluid velocity is generally lower in comparison to larger channels or pipes. Lower velocity is commonly linked to laminar flow, whereas higher velocities are more prone to inducing turbulent flow. Additionally, the smaller dimensions of mini-channels often contribute to the promotion of laminar flow.

Assuming that the flow conditions are incompressible, stable, two-dimensional, homogeneous, and laminar, the steady-state conservation equations are written as follows: (Szabo & Früh, 2017; Bezaatpour and Goharkhah 2019a,b, 2020):

Continuity equation

$$\boldsymbol{\nabla}.\left(\rho_{nf}\boldsymbol{u}\right) = 0 \tag{8}$$

Momentum equation

$$\boldsymbol{\nabla}.\left(\rho_{nf}\boldsymbol{u}\boldsymbol{u}\right) = -\boldsymbol{\nabla}P + \boldsymbol{\nabla}.(\bar{\bar{\tau}}) + \boldsymbol{F}_k \tag{9}$$

Energy equation

$$\boldsymbol{\nabla}.\left(\rho_{nf}\boldsymbol{u}C_pT\right) = \boldsymbol{\nabla}.\left(k_{nf}\,\boldsymbol{\nabla}\,T\right) \tag{10}$$

where $\bar{\bar{\tau}}$ is the stress tensor:

$$\bar{\bar{\tau}} = \mu_{nf}\left((\boldsymbol{\nabla}\,\boldsymbol{u} + (\boldsymbol{\nabla}\,\boldsymbol{u})^t) - \frac{2}{3}\boldsymbol{\nabla}.\boldsymbol{u}\,\delta_{ij}\,\bar{\bar{\mathrm{I}}}\right) \tag{11}$$

2.3 Boundary Conditions

a. Inlet Condition:

The inlet velocity is determined in terms of nanofluid features and the Reynolds number, the inlet temperatures are $T_0 = 293\mathrm{K}$.

b. Outlet Condition:

The outlet pressure is equivalent to atmospheric pressure.

c. The Walls Conditions:

The temperature continuity and no-slip boundary conditions are assumed at all fluid-solid interfaces. The bottom surface temperatures are $T_h = 350\mathrm{K}$.

2.4 Thermophysical Properties (Koo and Kleinstreuer 2004; Bezaatpour and Goharkhah 2019a, b, 2020):

Density

$$\rho_{nf} = (1-\varphi)\rho_f + \varphi\,\rho_p \tag{11}$$

Specific heat capacity

$$(\rho C_p)_{nf} = (1-\varphi)(\rho C_p)_f + \varphi(\rho C_p)_p \tag{12}$$

Dynamic viscosity

$$\mu_{nf} = \mu_f(1+2.5\varphi) \tag{13}$$

Electrical conductivity

$$\sigma_{nf} = \sigma_f\left[1 + \frac{3\left(\frac{\sigma_{np}}{\sigma_f}+1\right)\varphi}{\left(\frac{\sigma_{np}}{\sigma_f}+2\right) - \left(\frac{\sigma_{np}}{\sigma_f}-1\right)\varphi}\right] \tag{14}$$

Thermal conductivity

$$k_{nf} = k_{Static} + k_{Brownian} \tag{15}$$

$$k_{Static} = k_f\left[\frac{(k_p+2k_f) - 2\varphi(k_f-k_p)}{(k_p+2k_f) + 2\varphi(k_f-k_p)}\right] \tag{16}$$

$$k_{Brownian} = 5.10^4\beta\varphi\rho_f C_{p,f}\sqrt{\frac{kT}{\rho_p D_p}}.g(\varphi,T) \tag{17}$$

$$g(\varphi,T) = (-6.04\varphi + 0.4705)T + 1722.3\varphi - 134.63 \tag{18}$$

Where the indices f, p and nf denote respectively the basic fluid, the nanoparticles and the nanofluid, respectively.

2.5 The Generation of Entropy

Entropy generation rate resulting from heat transfer (Nguyen et al., 2020):

$$\mathcal{s}_{HT} = \frac{k_{nf}}{T^2}\left[\left(\frac{\partial T}{\partial x}\right)^2 + \left(\frac{\partial T}{\partial y}\right)^2\right] \tag{19}$$

Entropy generation rate resulting from friction:

$$\mathcal{s}_F = \frac{\mu_{nf}}{T}\left[2\left(\frac{\partial u}{\partial x}\right)^2 + 2\left(\frac{\partial v}{\partial y}\right)^2 + \left(\frac{\partial u}{\partial y} + \frac{\partial v}{\partial x}\right)^2\right] \tag{20}$$

Entropy generation rate resulting from the magnetic field:

$$\mathcal{s}_M = \frac{\sigma_{nf}{B_0}^2{U_{in}}^2}{T} \tag{21}$$

Total entropy generation (S):

$$S_{HT} = \int \mathcal{s}_{HT}\,d\mathcal{v} \tag{22}$$

$$S_F = \int \mathcal{s}_F\,d\mathcal{v} \tag{23}$$

$$S_M = \int \mathcal{s}_M\,d\mathcal{v} \tag{24}$$

$$S = S_{HT} + S_F + S_M \tag{25}$$

Table 2 Study of mesh sensitivity for $B = 800G, Re = 150$ et $\varphi = 2\%$

Number of grid (X×Y)	20×250	30×250	40×250	50×250	60×250
Nu_{Avg}	14.35	14.12	14.02	13.98	13.96
Relative error (%)	–	1.6	0.7	0.28	0.14

2.6 Heat Transfer and Hydrodynamic Parameters

Bejan number (Hussain et al., 2016):

$$Be = \frac{S_{HT}}{S} \tag{26}$$

Reynolds number (Ibrahim et al., 2021):

$$R_e = \frac{\rho_{nf} U_{in} D_h}{\mu_{nf}} = \frac{\rho_{nf} U_{in} D}{\mu_{nf}} \tag{27}$$

Local Nusselt number (Ibrahim et al., 2021):

$$Nu(x) = \frac{h(x) D_h}{k_{nf}} = \frac{h(x) D}{k_{nf}} \tag{28}$$

Average Nusselt number (Ibrahim et al., 2021):

$$Nu_{avg} = \frac{1}{L} \int_0^L Nu \, dx \tag{29}$$

The dimensionless temperature of the fluid:

$$\theta = \frac{T - T_0}{T_h - T_0} \tag{30}$$

2.7 Numerical Procedure

In our numerical study we have used a Fluent R1 calculation code, Fluent R1 user's guide (2019). The finite volume method is used to solve the governing equations. An uniform structured mesh is applied for all directions as shown in Fig. 2. For the pressure-velocity coupling, the SIMPLE algorithm is applied and a second-order upwind scheme is used for the quantity equations of movement and energy. To ensure the simulation accuracy, residual levels of 10E−6 are applied for the velocity and energy equations.

2.8 Grid Independence and Validation

The necessary step before doing any research during a numerical work is the parameterization which consists in ensuring that the results obtained are precise and independent of the number of nodes which form a calculation grid. Thus, different meshes were carried out in order to optimize and find the most appropriate mesh.

The results presented in Tab.1 show that from a grid system (50×250) in the directions $(x \times y)$, respectively, the numerical solution becomes independent of the cell size; in which the relative error of the mean Nusselt number is less than 1% from the mesh (40×250).

2. 9 Validations

Confirming the reliability of all CFD codes is an important part of any numerical simulation. To this end, we have taken several works from the literature and compared them with the results that we have found.

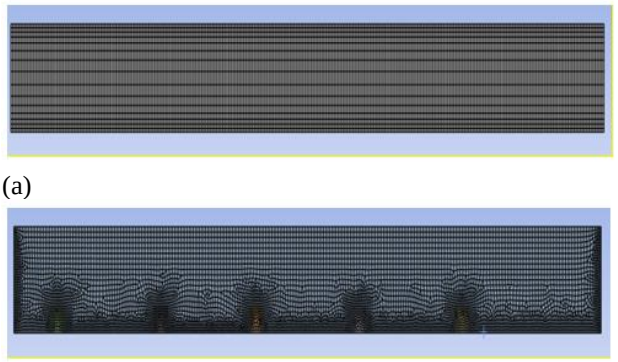

(a)

(b)

Fig. 2 Mesh of the studied configurations, (a): channel without fins; (b): channel with fins.

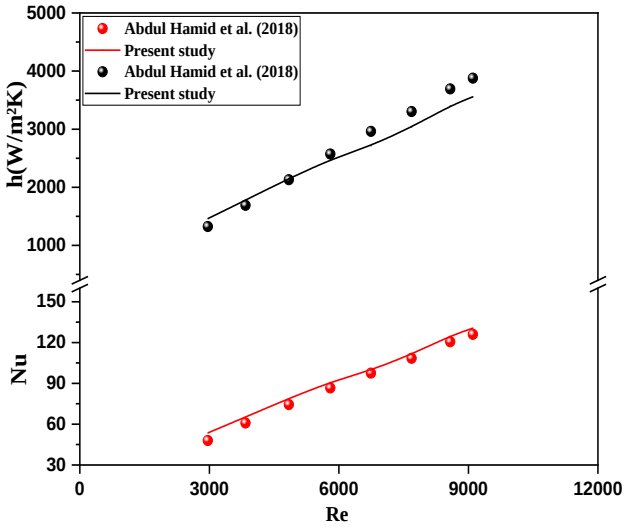

Fig. 3 Comparison of the heat transfer coefficient and Nusselt number predicted numerically to that measured experimentally by Hamid et al. (2018) for $T = 30°C$ with a 50: 50 mixing ratio

Validation 1

Hamid et al. (2018) have experimentally investigated the thermal performance of nanofluids (TiO_2/SiO_2) dispersed in a mixture $(water/ethylene\ glycol)$. A comparison is given in Fig. 3, for the convective heat transfer coefficient and Nusselt number obtained numerically and those experimentally.

Validation 2

Lajvardi et al. (2010) carried out an experimental study of the convective heat transfer of a ferrofluid flowing in a copper tube heated in the laminar regime in the presence of a magnetic field. The comparison of temperature profiles at different magnetic field intensities found numerically and experimentally is shown in Fig. 4.

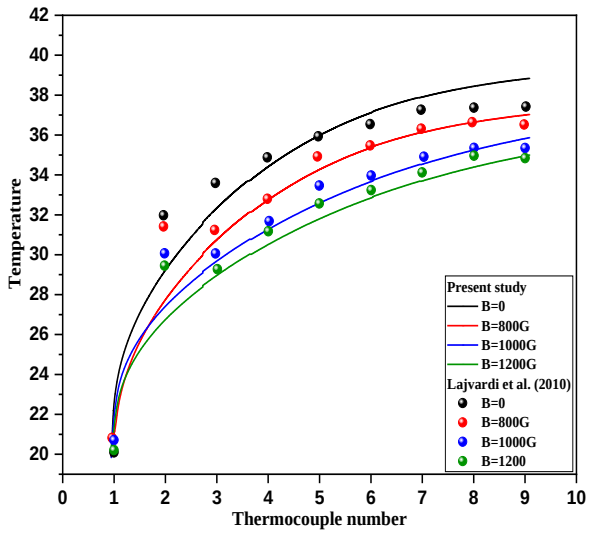

Fig. 4 Comparison of the temperature evolution for different values of magnetic field B (G) for $\varphi = 2.5\%$ predicted numerically to that measured experimentally by Lajvardi et al. (2010)

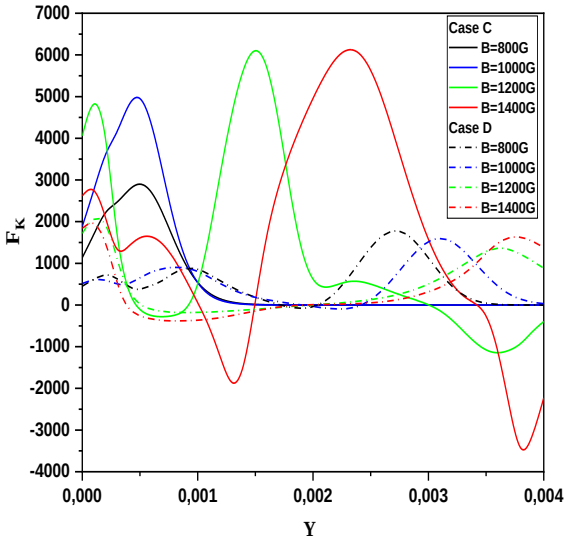

Fig. 5 Magnetic force variation at Re=150, and φ = 2%, $x_1 = 0.006$ m

At the end of this comparative study, this numerical method appears capable of reproducing good consistency between the results of the previous work and our results. Consequently, it can reliably simulate the various cases that will be discussed in this study.

3 RESULTS AND DISCUSSION

3.1 Effect of Magnetic Field Intensity

Ferrofluids are colloidal suspensions of magnetic nanoparticles in a carrier liquid. The presence of magnetic nanoparticles makes ferrofluids sensitive to magnetic fields and generates a magnetic body force when subjected to an external magnetic field. This magnetic body force can significantly influence the flow behavior of ferrofluids. Indeed, magnetic nanoparticles tend to accumulate in regions of high magnetic field intensity, orienting themselves in the direction of the field and forming aligned chains or aggregates. This alignment creates an increase in the overall magnetic force exerted on the ferrofluid. These magnetic chains can affect the ferrofluids resistance to flow and modify its viscosity and density.

The presence of the fins disturbs and modifies the flow of ferrofluid through them, promoting mixing (low thermal gradient), and disrupting the alignment and formation of the magnetic chains mentioned above. As a result, the magnetic force is attenuated (Fig. 5).

Figure 6 presents the evolution of the streamlines and the isotherms for various magnetic field intensities and for various studied configurations (A , B, C) and D. This figure presents the vortex formation mechanisms observed for the configurations (B), (C) and (D), with the exception of the configuration (A) where the flow is stable. For the configuration (B) ; the fins are obstacles which slow down and disturb the flow of the fluid and make the streamlines deviate upwards. This behavior leads to the small zones formation of stagnation and recirculation respectively upstream and downstream of each fin. On the other hand, in configuration (C), the

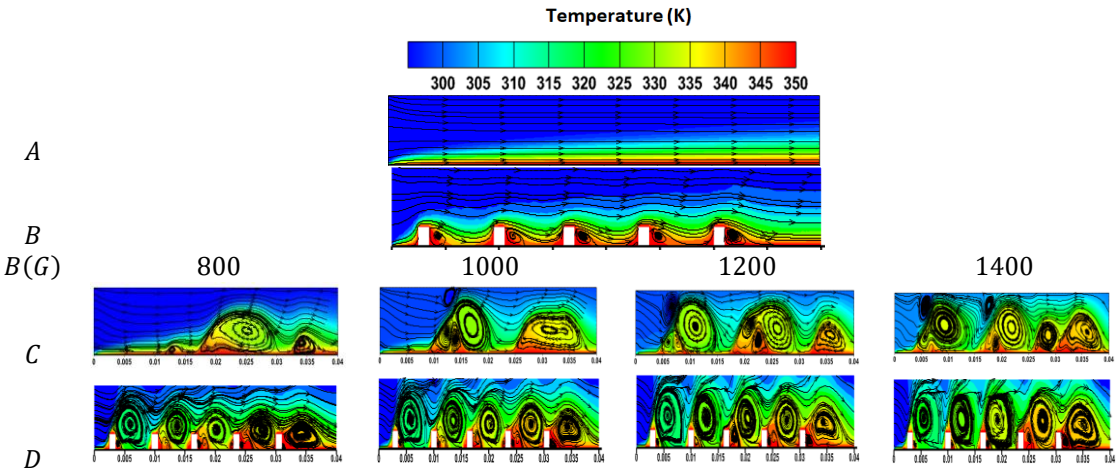

Fig. 6 Streamlines and temperature distribution for different cases and different magnetic field intensity at $Re = 150$ and $\varphi = 2\%$

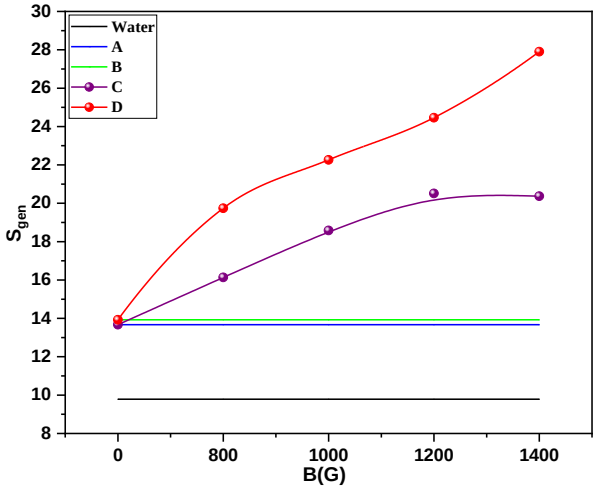

Fig. 7 Variation of Generated entropy versus magnetic field intensity for different cases at $Re = 150$ and $\varphi = 2$ %.

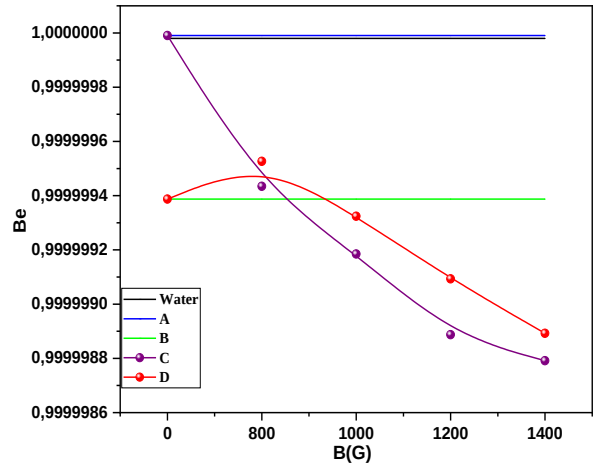

Fig. 8 Variation of Bejan number versus magnetic field intensity for different cases at $Re = 150$ and $\varphi = 2$ %

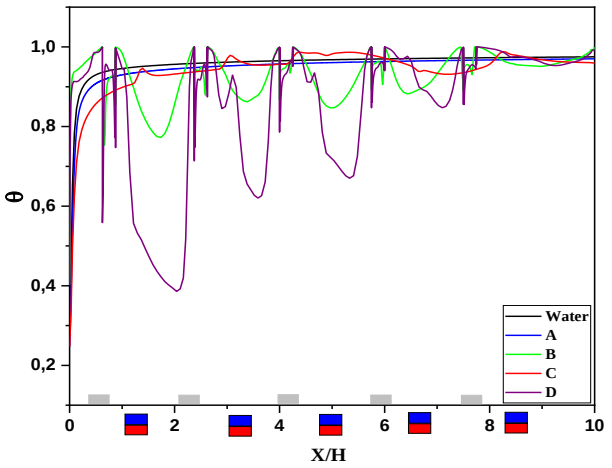

Fig. 9 Dimensionless temperature variation along the channel as a function of magnetic field intensity B for different cases at $Re = 150$ and $\varphi = 2$ %

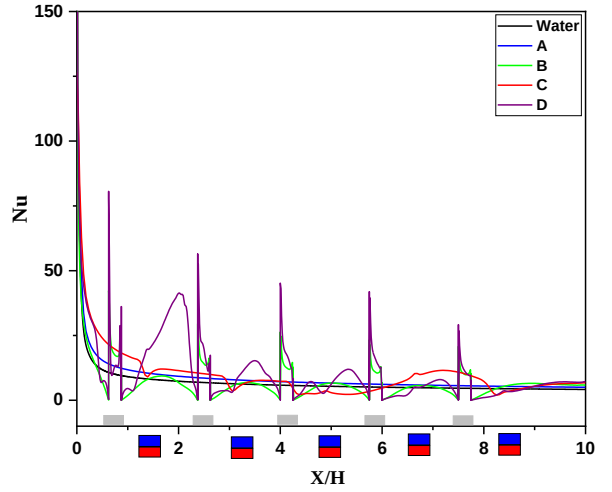

Fig. 10 Local Nusselt number variation as a function of magnetic field intensity B for different cases at $Re = 150$ and $\varphi = 2$ %

formation of the recirculation zone (vortex) is attributed to the upward magnetic force generated by the temperature gradient and the magnetic field produced by the pairs of magnets. just above of the hot wall. For configuration (D) where both types of vortex generators; the fins and the magnetic field, coexist together, there is an additional irregularity which favors the fusion of the vortices described above for the configurations (B) and (C), thus giving large cells close to the hot wall.

Figures 7 and 8 present the evolution of the entropy generated (S) and of the Bejan number (Be), respectively, versus the magnetic field intensity B for different configurations considered with $Re = 150$ and $\varphi = 2$ %.

Figure 7 illustrates that both the inclusion of fins and the introduction of a magnetic field act as disruptive factors in the flow. Indeed, each of its two parameters contributes effectively to the generation of entropy. Moreover, examination of this figure shows that as the magnetic field strength increases in the presence of fins, leads to an additional disturbance of the flow of the ferrofluid by effectively favoring the generation of total entropy.

The quantification of the contribution to entropy generation attributed to the magnetic field, S_{genM}, in comparison to the fluid friction S_{genF} and heat transfer S_{genT} is given by the number of Bejan (Be) presented on Fig. 8. The evolution of this parameter versus the magnetic field intensity reflects an increasing contribution from the magnetic field S_{genM} and of the viscosity S_{genF}. In this sense, the rate of irreversibility due to the thermal agitation gradually decreases following the intensification of the magnetic field while remaining dominant in front of the magnetic and viscous one.

To provide a quantitative description of the thermal aspects, we have presented in Figs 9 and 10 the longitudinal evolution of the dimensionless temperature and the local Nusselt number for different studied configurations, with a volume fraction and a Reynolds number $\varphi = 2$ % $Re = 150$. Without a magnetic field, the temperature (θ) undergoes a gradual rise, as a result

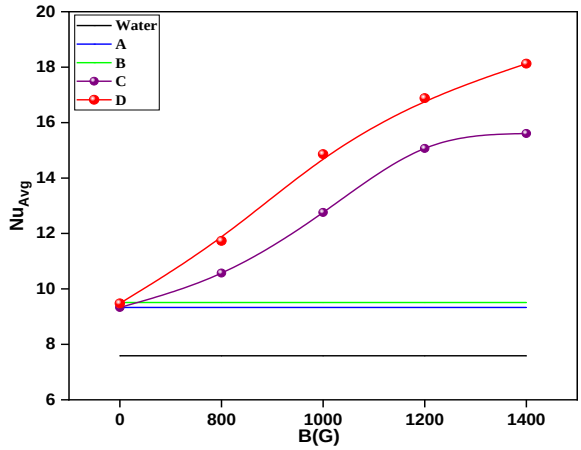

Fig. 11 Average Nusselt number as a function of magnetic field intensity B for different cases at $Re = 150$ and $\varphi = 2$ %

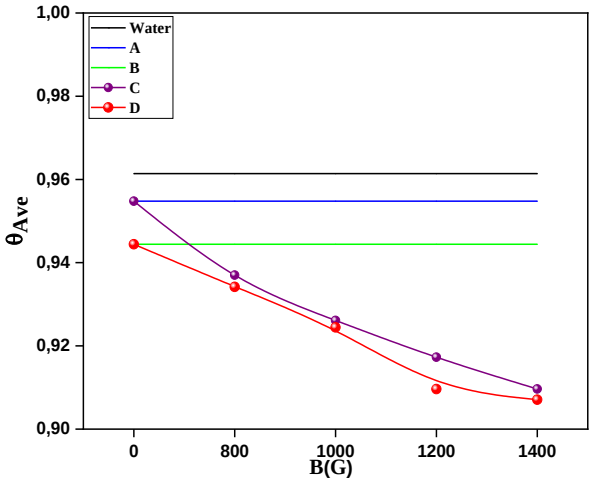

Fig. 12 Average dimensionless temperature as a function of magnetic field intensity B for different cases at $Re = 150$ and $\varphi = 2$ %

of heat transfer occurring between the hot wall and the cold ferrofluid. Additionally, one can observe that θ exhibits increases in proximity to the positions of the fins and permanent magnets in ($case\ B$) and ($case\ C$). It's important to highlight that these temperature peaks are related to the vortices created just above the hot mini-channel surface. However, in the presence of the two generators, the neighboring vortices created respectively undergo a fusion and finish to give a large vortex. In these regions, there are strong drops in temperature which gradually decrease along the channel. the decreases (minimums) of temperature in these regions are linked to a strong penetration of cold ferrofluids heading towards the hot wall which comes to lick it and extract heat there is thus a strong intensification of the rate of the transfer and subsequently, the maxima of the Nusselt number observed in these same regions (Fig. 10) For configuration without a magnetic field, Fig. 10 indicates a gradual decrease in the Nusselt number as the thickness of the thermal boundary layer (Fig. 6). Additionally, the curves obtained exhibit varying peaks

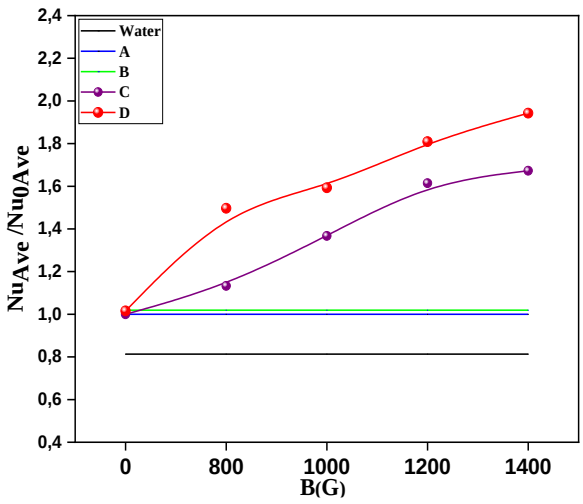

Fig. 13 Investigation of Nusselt number ratio as a function of magnetic field intensity B for different cases at $Re = 150$ and $\varphi = 2$ %

and troughs. This phenomenon can be attributed to the existence of vortices above the lower surface of the mini-channel, causing the thermal boundary layer to cyclically thicken and thin. It is shown that the presence of the magnetic sources leads to the migration of the nanoparticles Fe_3O_4 towards the heated wall; this conducts to an increase in the local thermal conductivity and, consequently, an enhancement in heat transfer in this region.

The Figs 11 et 12 illustrate the impact of the magnetic field intensity on the dimensionless temperature and the average Nusselt number respectively, for the different configurations. However, these figures clearly show a marked improvement in the heat transfer, which is coupled with a cooling of the hot wall for the different configurations compared to that of pure water. In the presence of fins ($Case\ B$), a disturbance and an increase in the exchange surface leads to a slight increase in Nusselt number. After the magnetic sources are activated ($Case\ C$), downstream of this, there is a migration of the nanoparticles (Fe_3O_4) towards the heated wall, consequently resulting in a higher thermal conductivity in this area.

In the impact region of magnetic sources, the effect of upward magnetic force and the phenomenon of thermophoresis cause the migration of hot nanoparticles towards the cold zone of the flow and consequently a greater heat transfer. For the ($Case\ D$) where the coexistence of two disturbing parameters of the flow, (fins + magnetic sources), a considerable improvement of the heat transfer rate is observed.

In order to quantify the enhancement in the transfer rate observed when using the fins and the magnetic field separately and simultaneously, we have plotted in the Fig. 13 the evolution of the relative Nusselt number (compared to the configuration (A)), as a function of the intensity of the magnetic field for different configurations. The examination of this figure shows a maximum heat transfer rate improvement of 5%, 20%

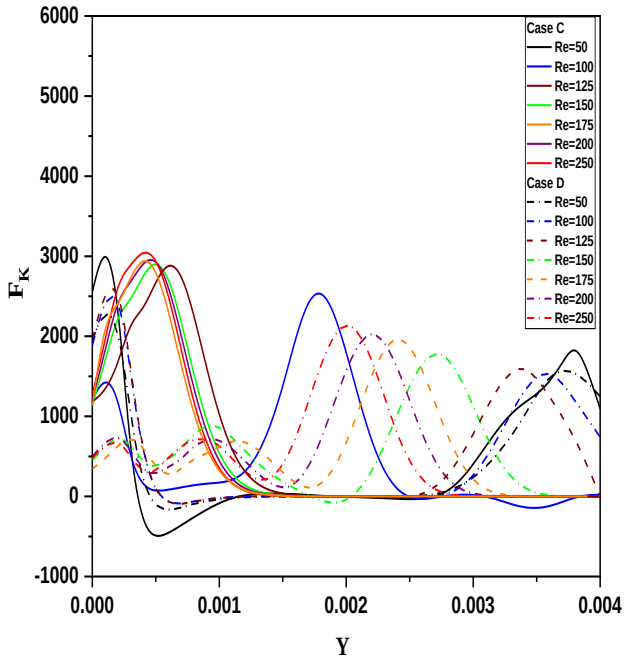

Fig. 14 Magnetic force variation for different Reynolds numbers at $B = 800$, and, $x_1 = 0.006$ m

and50% for the configurations (B), (C) and (D), respectively. Likewise for $B = 1400G$ this ratio achieved 67% and 99% for the configurations (C) and (D), respectively. Therefore, the configuration (D) is the most recommended for different magnetic field strength $B(G)$.

3.2 Effect of Reynolds Number Value

The transverse evolution of the body magnetic force without fins $(Case\ C)$ and with fins $(Case\ D)$ for different Reynolds number values is reported in Fig. 14. The results show that following an increase in Reynolds number, there is competition between two effects: an accelerating effect (Reynolds number) with a decelerating effect (fins). As a result, a clear attenuation of the effect of fins on body magnetic force is observed. It is conducted that the magnetic force continues to persist and exerts its strong effect on the upper part of the channel cross-section.

Figure 15 presents the isotherms and the streamlines in a minichannel for the different studied cases. This figure shows that following an increase in the Reynolds number Re, the extent of the domain which illustrates the cold fluid becomes larger, resulting in a considerable reduction in the vortices size which form just above the hot wall. Therefore, an attenuation of the magnetic field effect is observed following an acceleration of the flow.

Examination of this figure also shows that the use of the fins under the impact of a magnetic field for lower values of the Reynolds number promotes mixing and leads to the formation of high-intensity vortices entirely occupying the section of the channel. These large size vortices lead to blockage of the flow. As hydrodynamics and heat transport are closely related, this behavior thus results in a relatively low rate of heat transfer by convection.

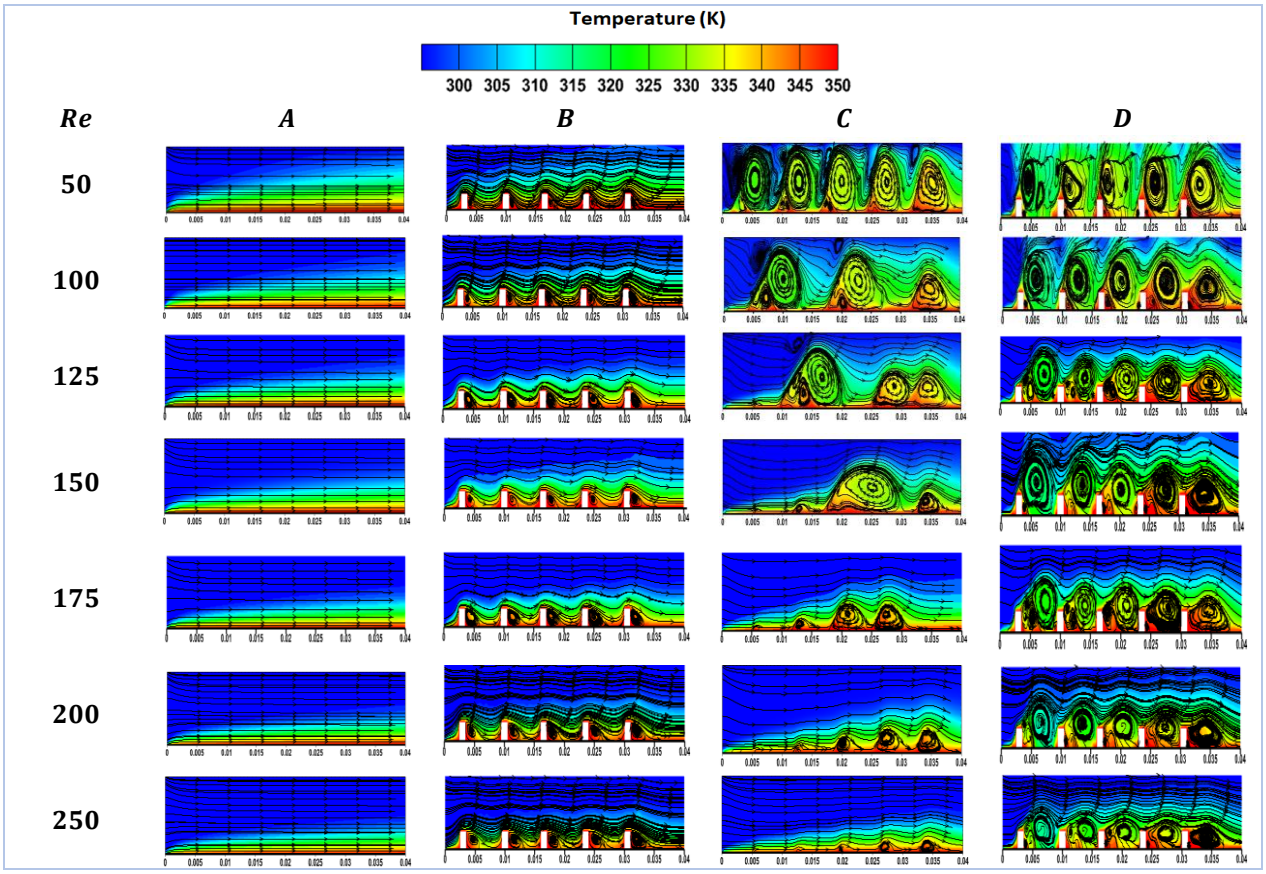

Fig. 15 Streamlines and temperature distribution for different cases and for different Reynolds number Re at $B = 800\ G$

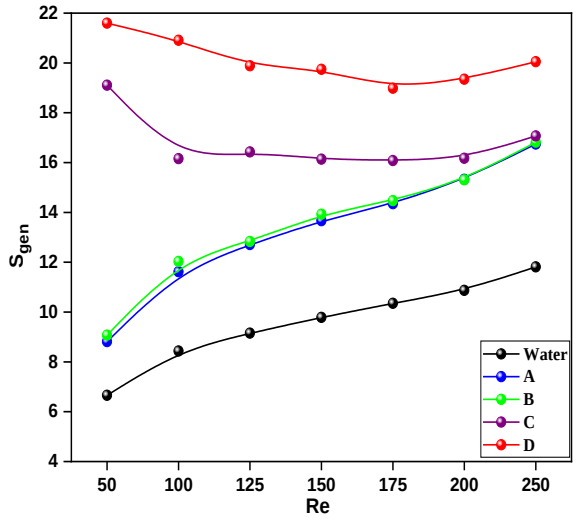

Fig. 17 Generated entropy variation as a function Reynolds number for different cases at $B = 800G$ and $\varphi = 2$ %

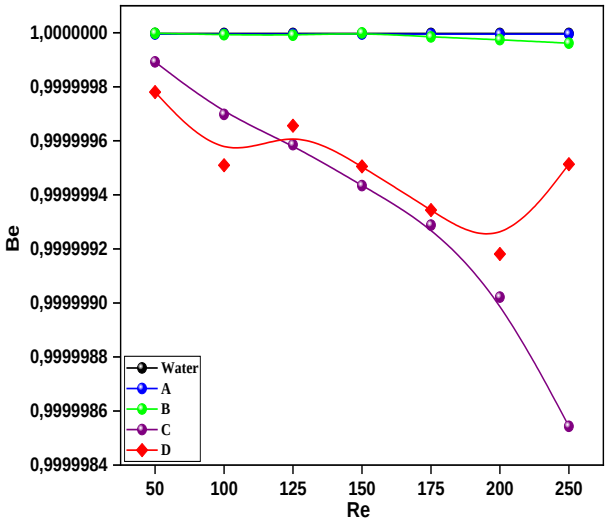

Fig. 18 Bejan number variation as a function of Reynolds number for different cases at $B = 800G$ and $\varphi = 2$ %

This figure also shows that the use of the fins under the impact of a magnetic field for lower values of the Reynolds number promotes mixing and leads to the formation of high-intensity vortices entirely occupying the section of the channel. These large size vortices lead to blockage of the flow. As hydrodynamics and heat transport are closely related, this behavior thus results in a relatively low rate of heat transfer by convection.

The Figs 17 and 18 illustrate the variations of the total entropy generation rate and the Bejan number, respectively, versus the Reynolds number for the different configurations with $B = 800G$ and $\varphi = 2\%$. it can be observed that the introduction of a magnetic field leads to a reduction in total entropy generation as the Reynolds number rises. This is caused by the decreasing of magnetic irreversibility with the significant improvement in flow velocity. However, with the absence of the magnetic field and with the presence of the fins, the total entropy generation rate increases as the Reynolds number increases due to the enhancement of frictional entropy generation. Moreover, the total entropy generation becomes maximal for low Reynolds numbers for the configurations (C) and (D). However, when the ferrofluid flows at higher velocities, the duration of its exposure to the magnetic field decreased. As a result, the magnetic field exerts a more significant influence on entropy generation at lower Reynolds numbers.

In addition, Fig. 18 shows, for the configurations without a magnetic field, the Bejan number (Be) remains unchanged, which explains that the contribution of the irreversibility due to the friction of the fluid S_{genF} becomes independent of the Reynolds number. In the presence of the magnetic field, the Bejan number gradually decreases. This reduction translates the increase in the contribution of the generation of entropy due to the magnetic field S_{genM} and that due to the friction of the fluid S_{genF}. By examining the configurations (C) and (D), it can be seen that the presence of the fins, which increases the heat exchange surface, promotes thermal irreversibility, thus leading to a slight increase in the Bejan number (configuration (D)).

The Figs 19 et 20 illustrate the variation of the average Nusselt number and the dimensionless temperature as a function of the Reynolds number for different configurations with magnetic field intensity $B = 800G$ and a volume fraction $\varphi = 2\%$.

These figures show that the heat transfer rate improves with the presence of the cold ferrofluid, following an increase in the Reynolds number for the different cases except for the configuration (C) where an opposite trend is observed. This behavior is the result of the increase in the speed of the flow which reduces the time during which the ferrofluid remains under the impact of the magnetic field. This leads to a reduction in the extent of the vortex and consequently the heat transfer rate decreases. There is a marked enhancement in the transfer rate for the configuration (D) in the presence of two vortex generators.

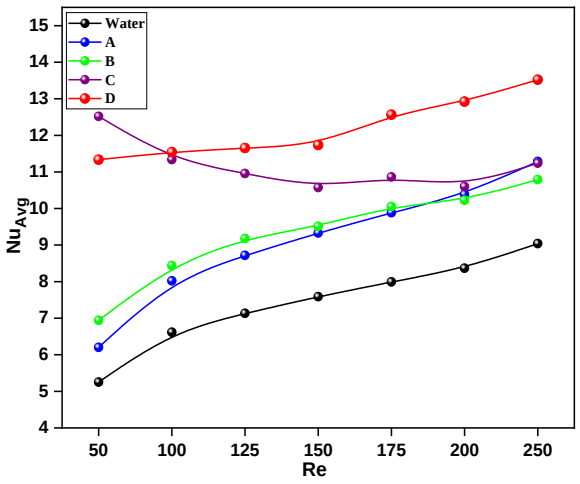

Fig. 19 Variation of the average Nusselt number versus Reynolds number for different cases at $B = 800G$ and $\varphi = 2$ %

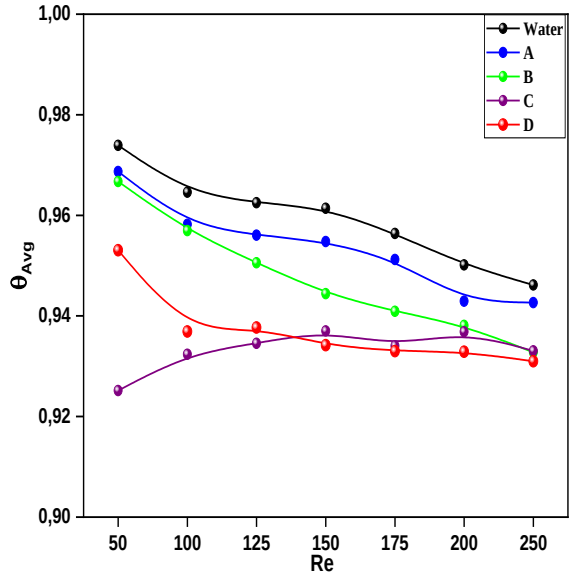

Fig. 20 Average dimensionless temperature as a function of Reynolds number Re for different case at $B = 800G$ and $\varphi = 2$ %

As shown in Fig. 21, the variation of relative Nusselt number versus the Reynolds number for different configurations with magnetic field strength $B = 800G$ and a volume fraction $\varphi = 2\%$. The obtained results show a greater value in the presence of magnetic Fe_3O_4 nanoparticles. So, the improvement of the heat transfer rate is obtained when the magnetic field is taken into account. It is also noted that the ratio decreases with increasing Reynolds number. This behavior is linked to a competition between the magnetic effect and the hydrodynamic effect. In particular, high values are observed for $Re = 50$ respectively $1.05, 1.85$ and 2 for configurations$(B), (D)$ and(C), this means that the use of low Reynolds number leads to an optimal thermal performance factor.

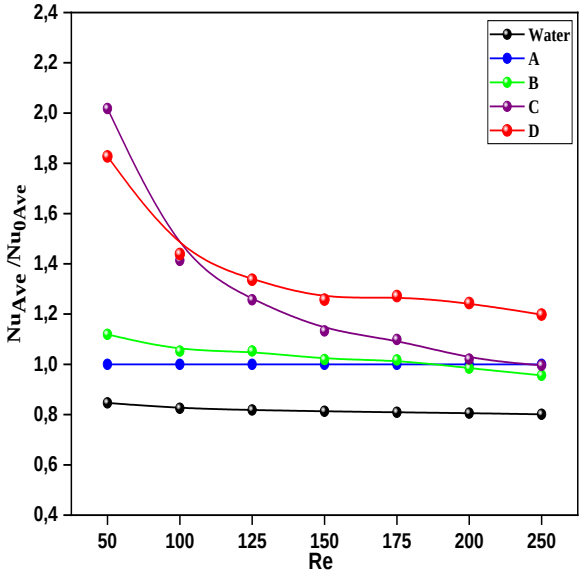

Fig. 21 Investigation of Nusselt number ratio as a function of Reynolds number Re for different cases at $B = 800G$ and $\varphi = 2$ %

Moreover, a comparison between the different configurations makes it possible to highlight a considerable improvement in heat transfer rate and those in the presence of the two vortex generators simultaneously $(Case\ D)$.

4 Conclusions

The heat transfer by convection of a laminar flow of a ferrofluid in a channel subjected to a constant temperature numerically has been carried out. The main findings of the ongoing investigation are listed below:

- The use of fins causes recirculation zones to form downstream of the fins and become larger and stronger with increasing Reynolds number. These vortices have a crucial role in the generation of entropy and consequently the enhancement of heat transfer, as they promote the migration of nanoparticles from the hot bottom surface to cooler regions, which increases the heat transfer.
- The presence of magnetic sources stimulates the appearance of recirculation zones (vortices), just above the hot wall. The size of these cells increases with increasing magnetic field strength and decreasing Reynolds number. Also the magnetic effect promotes mixing and leads to additional irreversibility, thus resulting in a significant improvement in heat transfer.
- The coexistence of the magnetic field and the fins leads to the fusion of the vortices created by these two vortex generators and consequently an increase in the mixing of the ferrofluid which promotes the heat transfer rate.
- The presence of the fins and the magnetic field reinforce the periodic attraction of the cold ferrofluid towards the heated surface and its subsequent release in the direction of the main flow of the flow, thus disturbing the thermal boundary layer which promotes mixing and increasing heat transfer.

  It is beneficial to use fins and magnetic sources simultaneously (Case D), with an intense magnetic field and a low Reynolds number in order to ensure a large gain in heat transfer.

  In future work, we want to deepen our study by highlighting other parameters that intervene and affect the performance of the exchange, which include; the orientation of the magnetic field, the number of magnet pairs, and the volume fraction of magnetic nanoparticles...etc.

ACKNOWLEDGMENT

The authors express their sincere gratitude to the reviewers for their invaluable comments and suggestions. Additionally, they extend their appreciation to Professors Bechir MOUSSA, Lobna BEN SALEM, and Nawel DJOBBI for their meticulous review and enhancements to the manuscript's English language.

CONFLICT OF INTEREST

The authors declare that they have no known competing financial interests or personal relationships that could have appeared to influence the work reported in this paper.

AUTHORS CONTRIBUTION

Laila Boutas: Data organization, Writing- Original draft preparation; **Mbarek Marzougui**: Investigation, Reviewing, and Editing; **Jamil Zinoubi**: Conceptualization, Methodology, Software, and Supervision; **Soufien Gannouni**: Software, Validation

REFERENCES

Akbari, O. A., Toghraie, D., & Karimipour, A. (2015). Impact of ribs on flow parameters and laminar heat transfer of water–aluminum oxide nanofluid with different nanoparticle volume fractions in a three-dimensional rectangular microchannel. *Advances in Mechanical Engineering*, *7*(11), 1687814015618155. https://doi.org/10.1177/1687814015618155

Amani, M., Ameri, M., & Kasaeian, A. (2018). Hydrothermal assessment of ferrofluids in a metal foam tube under low-frequency magnetic field. *International Journal of Thermal Sciences*, *127*, 242-251. https://doi.org/10.1016/j.ijthermalsci.2018.01. 031

Aminfar, H., Mohammadpourfard, M., & Zonouzi, S. A. (2013). Numerical study of the ferrofluid flow and heat transfer through a rectangular duct in the presence of a non-uniform transverse magnetic field. *Journal of Magnetism and Magnetic materials*, *327*, 31-42. https://doi.org/10.1016/j.jmmm.2012. 09.011

ANSYS Fluent Tutorial Guide, R1, ANSYS, Inc, Canonsburg, PA, January 2019.

Azizian, R., Doroodchi, E., McKrell, T., Buongiorno, J., Hu, L. W., & Moghtaderi, B. (2014). Effect of magnetic field on laminar convective heat transfer of magnetite nanofluids. *International Journal of Heat and Mass Transfer*, *68*, 94-109. https://doi.org/10.1016/j.ijheatmasstransfer.2013.09.011

Bezaatpour, M., & Goharkhah, M. (2019a). A novel heat sink design for simultaneous heat transfer enhancement and pressure drop reduction utilizing porous fins and magnetite ferrofluid. *International Journal of Numerical Methods for Heat & Fluid Flow*, *29*(9), 3128-3147. https://doi.org/10.1108/HFF-12-2018-0810

Bezaatpour, M., & Goharkhah, M. (2019b). Effect of magnetic field on the hydrodynamic and heat transfer of magnetite ferrofluid flow in a porous fin heat sink. *Journal of Magnetism and Magnetic Materials*, *476*, 506-515. https://doi.org/10.1016/j.jmmm.2019.01.028

Bezaatpour, M., & Goharkhah, M. (2020). A magnetic vortex generator for simultaneous heat transfer enhancement and pressure drop reduction in a mini channel. *Heat Transfer*, *49*(3), 1192-1213. https://doi.org/10.1002/htj.21658

Ganguly, R., Sen, S., & Puri, I. K. (2004a). Heat transfer augmentation using a magnetic fluid under the influence of a line dipole. *Journal of Magnetism and Magnetic Materials*, *271*(1), 63-73. https://doi.org/10.1016/j.jmmm.2003.09.015

Ganguly, R., Sen, S., & Puri, I. K. (2004b). Thermomagnetic convection in a square enclosure using a line dipole. *Physics of Fluids*, *16*(7), 2228-2236. https://doi.org/10.1063/1.1736691

Ghale, Z. Y., Haghshenasfard, M., & Esfahany, M. N. (2015). Investigation of nanofluids heat transfer in a ribbed microchannel heat sink using single-phase and multiphase CFD models. *International Communications in Heat and Mass Transfer*, *68*, 122-129. https://doi.org/10.1016/j.icheatmasstransfer.2015.08.012

Ghofrani, A., Dibaei, M. H., Sima, A. H., & Shafii, M. B. (2013). Experimental investigation on laminar forced convection heat transfer of ferrofluids under an alternating magnetic field. *Experimental Thermal and Fluid Science*, *49*, 193-200. https://doi.org/10.1016/j.expthermflusci.2013.04.018

Gupta, M., & Kasana, K. S. (2012). Numerical study of heat transfer enhancement and fluid flow with inline common-flow-down vortex generators in a plate-fin heat exchanger. *Heat Transfer—Asian Research*, *41*(3), 272-288. https://doi.org/10.1002/htj.20414

Hamid, K. A., Azmi, W. H., Nabil, M. F., & Mamat, R. (2018). Experimental investigation of nanoparticle mixture ratios on TiO2–SiO2 nanofluids heat transfer performance under turbulent flow. *International Journal of Heat and Mass Transfer*, *118*, 617-627. https://doi.org/10.1016/j.ijheatmasstransfer.2017.11.036

Hussain, S., Mehmood, K., & Sagheer, M. (2016). MHD mixed convection and entropy generation of water–alumina nanofluid flow in a double lid driven cavity with discrete heating. *Journal of Magnetism and Magnetic Materials*, *419*, 140-155. https://doi.org/10.1016/j.jmmm.2016.06.006

Ibrahim, M., Saeed, T., Bani, F. R., Sedeh, S. N., Chu, Y. M., & Toghraie, D. (2021). Two-phase analysis of heat transfer and entropy generation of water-based magnetite nanofluid flow in a circular microtube with twisted porous blocks under a uniform magnetic field. *Powder Technology*, *384*, 522-541. https://doi.org/10.1016/j.powtec.2021.01.077

Karimipour, A., Alipour, H., Akbari, O. A., Semiromi, D. T., & Esfe, M. H. (2015). Studying the effect of indentation on flow parameters and slow heat transfer of water-silver nanofluid with varying volume fraction in a rectangular Two-Dimensional microchannel. *Indian Journal of Science and Technology*, *8*, 51707. http://dx.doi.org/10.17485/ijst/2015/v8i15/51707

Koo, J., & Kleinstreuer, C. (2004). A new thermal conductivity model for nanofluids. *Journal of Nanoparticle Research*, *6*, 577-588. http://dx.doi.org/10.1007/s11051-004-3170-5

Lajvardi, M., Moghimi-Rad, J., Hadi, I., Gavili, A., Isfahani, T. D., Zabihi, F., & Sabbaghzadeh, J. (2010). Experimental investigation for enhanced ferrofluid heat transfer under magnetic field effect. *Journal of Magnetism and Magnetic Materials*, *322*(21), 3508-3513. https://doi.org/10.1016/j.jmmm.2010.06.054

Manca, O., Nardini, S., & Ricci, D. (2012). Numerical study of nanofluid forced convection in ribbed channels. *Applied* Thermal *Engineering*, 37, 280-292. http://dx.doi.org/10.1016/j.applthermaleng.2011.11.030

Mechighel, F., El Ganaoui, M., Kadja, M., Pateyron, B., & Dost, S. (2009). Numerical simulation of three dimensional low Prandtl liquid flow in a parallelepiped cavity under an external magnetic field. *FDMP: Fluid Dynamics & Materials Processing*, *5*(4), 313-330. https://doi.org/10.3970/fdmp.2009.005.313

Motozawa, M., Chang, J., Sawada, T., & Kawaguchi, Y. (2010). Effect of magnetic field on heat transfer in rectangular duct flow of a magnetic fluid. *Physics Procedia*, *9*, 190-193. http://dx.doi.org/10.1016/j.phpro.2010.11.043

Mousavi, S. M., Biglarian, M., Darzi, A. A. R., Farhadi, M., Afrouzi, H. H., & Toghraie, D. (2019). Heat transfer enhancement of ferrofluid flow within a wavy channel by applying a non-uniform magnetic field. *Journal of Thermal Analysis and Calorimetry*, *139*, 3331-3343. https://doi.org/10.1007/s10973-019-08650-6

Nguyen, Q., Sedeh, S. N., Toghraie, D., Kalbasi, R., & Karimipour, A. (2020). Numerical simulation of the ferro-nanofluid flow in a porous ribbed microchannel heat sink: investigation of the first and second laws of thermodynamics with single-phase and two-phase approaches. *Journal of the Brazilian Society of Mechanical Sciences and Engineering*, *42*, 1-14. http://dx.doi.org/10.1007/s40430-020-02534-9

Pishkar, I., & Ghasemi, B. (2012). Cooling enhancement of two fins in a horizontal channel by nanofluid mixed convection. *International Journal of Thermal Sciences*, *59*, 141-151. https://doi.org/10.1016/j.ijthermalsci.2012.04.015

Ragoju, R., & Shekhar, S. (2020). Linear and weakly nonlinear analyses of magneto-convection in a sparsely packed porous medium under gravity modulation. *Journal of Applied Fluid Mechanics*, *13*(6), 1937-1947. 10.47176/jafm.13.06.31560

Sachdeva, G., Kasana, K. S., & Vasudevan, R. (2010). Heat transfer enhancement by using a rectangular wing vortex generator on the triangular shaped fins of a plate‐fin heat exchanger. *Heat Transfer—Asian Research: Co‐sponsored by the Society of Chemical Engineers of Japan and the Heat Transfer Division of ASME*, *39*(3), 151-165. https://doi.org/10.1002/htj.20285

Sadeghinezhad, E., Mehrali, M., & Akhiani, A. R. (2017). Experimental study on heat transfer augmentation of graphene based ferrofluids in presence of magnetic field. *Applied* Thermal *Engineering*, *114*, 415-427. https://doi.org/10.1016/j.applthermaleng.2016.11.199

Scherer, C., & Figueiredo Neto, A. M. (2005). Ferrofluids: properties and applications. *Brazilian journal of physics*, *35*, 718-727. https://doi.org/10.1590/S0103-97332005000400018

Sheikholeslami, M., & Ganji, D. D. (2017). Free convection of Fe3O4-water nanofluid under the influence of an external magnetic source. *Journal of Molecular Liquids*, *229*, 530-540. https://doi.org/10.1016/j.molliq.2016.12.101

Sheikholeslami, M., & Ganji, D. D. (2018). Ferrofluid convective heat transfer under the influence of external magnetic source. *Alexandria engineering journal*, *57*(1), 49-60. https://doi.org/10.1016/j.aej.2016.11.007

Sheikholeslami, M., Arabkoohsar, A., Khan, I., Shafee, A., & Li, Z. (2019). Impact of Lorentz forces on Fe3O4-water ferrofluid entropy and exergy treatment within a permeable semi annulus. *Journal of Cleaner Production*, *221*, 885-898. https://doi.org/10.1016/j.jclepro.2019.02.075

Sheikholeslami, M., Ellahi, R., & Vafai, K. (2018). Study of Fe3O4-water nanofluid with convective heat transfer in the presence of magnetic source. *Alexandria Engineering Journal*, *57*(2), 565-575. https://doi. org/10.1016/j.aej.2017.01.027

Szabo, P. S., & Früh, W. G. (2017). The transition from natural convection to thermomagnetic convection of a magnetic fluid in a non-uniform magnetic field. *Journal of Magnetism and Magnetic Materials*, *447*, 116-123. http://dx.doi.org/10.1016/j.jmmm.2017.09.028

Tari, I., & Mehrtash, M. (2013). Natural convection heat transfer from inclined plate-fin heat sinks. *International Journal of Heat and Mass Transfer*, *56*(1-2), 574-593.

http://dx.doi.org/10.1016/j.ijheatmass transfer. 2012.08.050.

Wang, C. C. (2005). Mixed convection boundary layer flow on inclined wavy plates including the magnetic field effect. *International Journal of Thermal Sciences*, *44*(6), 577-586. https://doi.org/10.1016/j.ijthermalsci.2005.02.001

Xuan, Y., Li, Q., & Ye, M. (2007). Investigations of convective heat transfer in ferrofluid microflows using lattice-Boltzmann approach. *International Journal of Thermal Sciences*, *46*(2), 105-111. https://doi.org/10.1016/j.ijthermalsci.2006.04.002